Experimental evidence for chiral melting of the Ge(113) and Si(113) 3×1 surface phases

J. Schreiner, K. Jacobi, and W. Selke*
Fritz-Haber-Institut der Max-Planck-Gesellschaft, Faradayweg 4-6, D-14195 Berlin, Germany
(Received 24 May 1993; revised manuscript received 20 September 1993)

Results of a spot-profile-analysis low-energy-electron-diffraction study of the 3×1 order-disorder phase transition of the Ge(113) and Si(113) surfaces are reported. For Ge(113) agreement with predictions for chiral melting with isotropic scaling is found. For Si(113) we compare our findings to those of other LEED and x-ray-scattering studies.

I. INTRODUCTION

During the past years there has been significant progress in the understanding of two-dimensional (2D) phase transitions described by Potts or clock models[1–5]. In particular, the transition from a (3×1) commensurate (C) phase to an incommensurate (IC) phase has been studied extensively.[6–14] Huse and Fisher[6,7] pointed out that the classification scheme used at that time was incomplete and suggested an additional universality class which was displayed, in a prototypical way, by the 2D three-state chiral clock model. In this universality class, a continuous transition directly from a C solid into an IC fluid may occur; this is called chiral melting.

Experimental evidence for such chiral melting is still rather scarce. Recently, Yang *et al.*[15] presented a spot-profile-analysis low-energy-electron-diffraction (SPA-LEED) study of the disordering of the Si(113) (3×1) reconstruction. Here, the reconstructed surface layer plays the role of the 2D system which undergoes phase transformations. The unreconstructed deeper layers may be considered as the substrate supplying adsorption sites. Yang *et al.* observed an asymmetric broadening and a shift away from the commensurate position for the 3×1 LEED spot. They argued that their findings on various critical exponents and the temperature dependence of the incommensurability are consistent with chiral melting.

In the course of a project on semiconductor (113) surfaces, we have studied the Si(113) surface in great detail with angle-resolved UV photoemission and high-resolution electron-energy-loss spectroscopy.[16–18] We found that at 300 K the surface has a 3×2 reconstruction which is easily transformed with many residual gases into a 3×1 structure. At the moment there is a majority of studies[16–22] which find a 3×2 structure at 300 K and a minority[15,23] which argue for a 3×1 structure. Despite two scanning-tunneling-microscopy (STM) studies,[22,23] the atomic structure of the Si(113) surface is not completely solved. Jacobi and Myler[18] have proposed a buckling model for the 3×2 structure which accounts for the observation that the 3×2 structure is easily transformed into a H-terminated (3×1)-H surface. The open question of the correct positions of the atoms prevents, at present, the elaboration of a realistic microscopic model for the (3×1) order-disorder phase transition. It does not prevent, however, the study of the classification of this transition. In view of the difficulties in preparing clean Si(113) surfaces we also have investigated Ge(113). It turned out that the experiments for Ge(113) give more convincing evidence for chiral melting with isotropic scaling than those for Si(113). After completion of our measurements, we were informed about an x-ray-scattering study for Si(113).[24] We will comment on that work in our discussion.

Our contribution is organized as follows: Experimental details are given in Sec. II, followed by the results in Sec. III and discussion in Sec. IV. We present and discuss the results for Si(113) and Ge(113) together.

II. EXPERIMENT

The experiments were performed in an UHV chamber with a base pressure of 4×10^{-11} mbar pumped by a turbomolecular pump and a Ti sublimation pump. We used a spot-profile-analysis LEED system with a transfer width better than 1000 Å. The boron-doped p-type silicon sample had a dopant concentration of 2.5×10^{17} cm^{-3} and a resistivity of 0.1 Ω cm^{-1}. The germanium sample was weakly n doped. Both samples had a size of $10\times7\times3$ mm^3.

The preparation of the Si(113) surfaces is described elsewhere.[16] Briefly, the silicon sample was polished with cerium oxide (0.25 μm granulation size). In a second polishing step a colloidal silicic acid dispersion (0.125 μm granulation size) was used, followed by an etching process with 40% hydrofluoric acid. Finally, the surface was covered with silicon oxide to avoid contamination during transfer to the UHV chamber and during the baking of the system. The Ge(113) surfaces were first mechanically polished with cerium oxide with a final granulation size of 0.25 μm. To remove the topmost damaged surface layers the sample was etched with HNO_3, HF, CH_3COOH 4:4:10. In a second step the germanium sample was treated with hot NaOCl to cover the surface with thin film of germanium oxide. The etching and oxidation steps were done three times. Each step took 5 min and was followed by a rinse in distilled water.

The sample was mounted at a tantalum block which could be pressed against a copper block to allow cooling either with liquid nitrogen (120 K) or with liquid helium (20 K). During heating the Ta block was separated from the copper block. The heating was performed from the

back side through a tungsten filament (250 W). The sample could be heated up to 1500 K through electron bombardment. The temperature distribution on the sample was very uniform because of the large mass of the tantalum block. The temperature was monitored with a Pt-Pt/Rh thermocouple for Si and a NiCr-CuNi thermocouple for Ge, which were welded to the Ta block beneath the sample. For temperatures above 700 K an infrared (IR) pyrometer was used to calibrate the thermocouple. For silicon the absolute-temperature measurement was accurate to within $\Delta T = \pm 20$ K. For germanium we calibrated the temperature by using the melting point at 1210.5 K. This reduced the uncertainty in temperature to $\Delta T = \pm 10$ K. The relative accuracy in temperature was ± 0.2 K.

After the base pressure had been reached in the UHV chamber, the sample and the Ta block were degassed for several hours with increasing temperature up to 850 K. When the pressure at this temperature was better than 1×10^{-10} mbar the sample was flashed to 1470 K for Si and to 1150 K for Ge to remove the thin oxide layer. During the flash the pressure stayed below 1×10^{-8} mbar. This procedure helped to reduce C contamination and reduced sputtering time. During a long period of measurement only flashing to 1470 K was sufficient to achieve a clean silicon surface. After flashing, the germanium sample was cleaned additionally by Ar^+ sputtering and annealing (1150 K) cycles.

III. RESULTS

A. LEED pattern and its temperature dependence: overview

A LEED pattern of the clean annealed Si(113) surface (Fig. 1) shows the known 3×2 reconstruction at 300 K.[16] One possible 1×1 unit cell in k space is drawn connecting 1×1 spots. The LEED pattern also exhibits 3×1 and 3×2 spots. All spots have a Gaussian line shape. The 1×1 and 3×1 spots have the same full width at half maximum corresponding to a correlation length of 250 Å, which is limited by defects and steps on the surface. The 3×2 superstructure spots are three times broader (75-Å correlation length) and have an intensity ten times smaller.

For Ge(113) we found a 3×2 superstructure similar to that of Si(113) (Fig. 2). The low temperature was necessary because the 3×2 superstructure spots are very weak and broad (40-Å correlation length only). Olshanetsky, Mashanov, and Nikiforov[25] found at room temperature only a 3×1 reconstruction. The Ge(113) 1×1 and 3×1 superlattice spots are sharper (370-Å correlation length) than the spots on the Si(113) surface. We could not find any change of the Ge(113) 3×2 reconstruction by the residual gas within four days. Since the contamination from residual gas was smaller and the ordered areas were larger, Ge(113) was more suitable for investigating the phase transition than Si(113).

For an overview we measured the temperature dependence of the integral intensities from a 3×1 and 3×2 LEED spot for Si(113) as shown in Fig. 3. The Si(113) 3×2 surface experiences a transition into a 3×1 reconstructed surface (full dots) which is completed at about 780 K. At $T_c \approx 929$ K the silicon surface undergoes an order-disorder phase transition from 3×1 into a 1×1 disordered surface. The determination of T_c is described below. Since the transition temperatures are quite different, the 3×2 reconstruction has no influence on the 3×1 order-disorder phase transition. For Ge(113) we found a similar temperature dependence for the 3×2 (full dots) and 3×1 (open dots) integral LEED intensities (Fig. 4). Compared to Si(113), the 3×2 LEED spots vanish at lower temperature (750 K) and the 3×1 spots disappear at higher temperature ($T_c \approx 1063$ K). Accordingly, the temperature window of the pure 3×1 reconstruction is

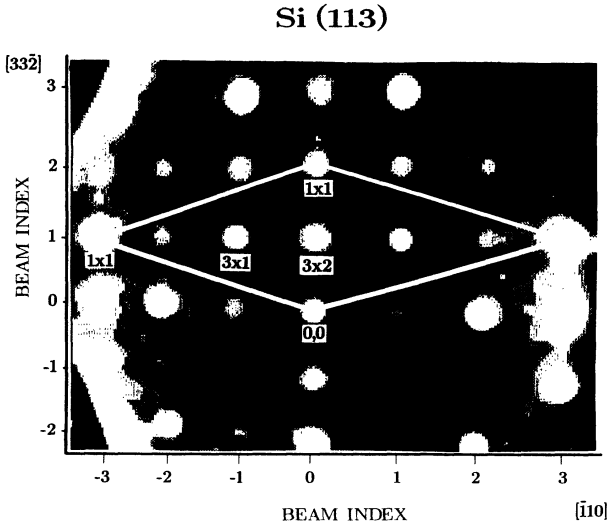

FIG. 1. LEED pattern of the 3×2 reconstructed Si(113) surface at room temperature ($E_p = 60$ eV) using a spot-profile-analysis system LEED (SPA-LEED).

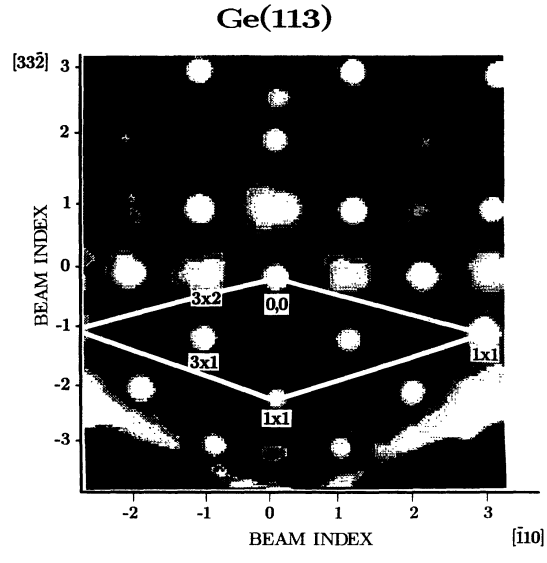

FIG. 2. LEED pattern of the 3×2 reconstructed Ge(113) surface at about 120 K ($E_p = 50$ eV). The 3×2 spots are three times broader and weaker than for the Si(113) surface.

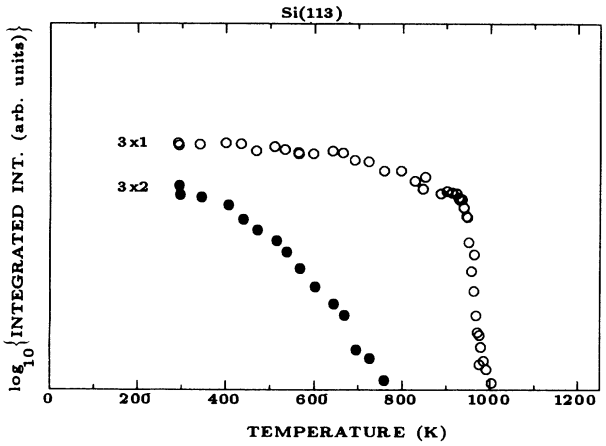

FIG. 3. Integrated intensities for two different spots of the Si(113) surface: For the 3×2 structure the $(\bar{3},\bar{3})$ spot and for the 3×1 structure the $(\bar{1},\bar{3})$ spot is chosen. $E_p=60$ eV.

larger than in the case of Si(113), and any anticipated influence of the 3×2 reconstruction on the 3×1 transition is expected to be weaker for Ge(113) than for Si(113). During the 3×1 phase transition the integral intensities of the 1×1 spots also decreased to an intensity which arises only from the scattering at second- and higher-order layers. At 1210.5 K the Ge(113) surface melts, as mentioned above, and the 1×1 LEED pattern disappears.

B. 3×1 order-disorder phase transition

We now present our data for the 3×1 order-disorder phase transition in detail. Close to the transition temperature T_c the 3×1 LEED spot intensities drop down to zero. Above T_c the 3×1 superlattice spots broaden and continuously move away from the commensurate $\frac{1}{3}$ position towards the $\frac{1}{4}$ position. This is shown in Fig. 5 for

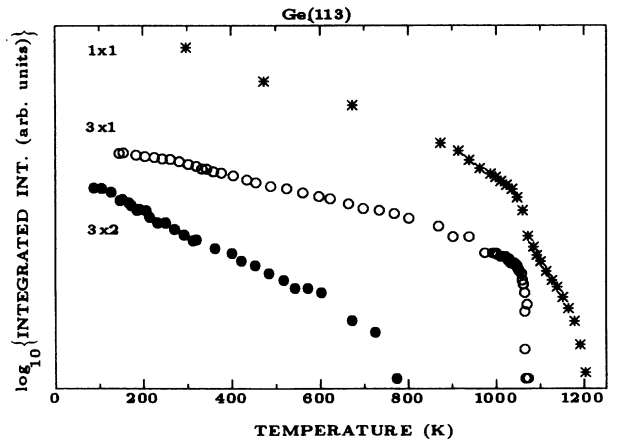

FIG. 4. Integrated intensities for three different spots of the Ge(113) surface: For the 3×2 structure the (0,1) spot and for the 3×1 structure the $(\bar{1},1)$ spot is chosen. The (0,2) spot belongs to the 1×1 substrate pattern. $E_p=50$ eV.

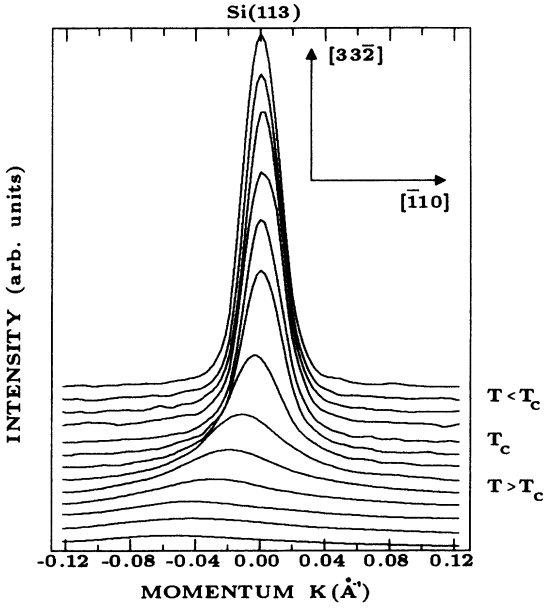

FIG. 5. LEED spot profiles in the $(\bar{1}10)$ direction of the Si(113) 3×1 $(\bar{1},1)$ superlattice spot for temperatures in the vicinity of the (3×1) order-disorder phase transition at T_c.

Si(113) 3×1. The same behavior is found for Ge(113). The $(\bar{1},1)$ reflex of Ge(113) is shown in a two dimensional plot in Fig. 6. At lower temperatures (a)–(c), the 3×1 LEED spot is at the $\frac{1}{3}$ position. For $T>T_c$ (d)–(f) the spot broadens strongly along the $(1\bar{1}0)$ direction and shifts along the $(1\bar{1}0)$ direction away from the commensurate position to larger values of the momentum k (smaller values of the relative momentum K in Fig. 6). The magnitude of this shift is independent of the beam index. The shift is always along the $(\bar{1}10)$ axis towards the nearest 1×1 spot.

The LEED intensity of a Si(113) 3×1 and Ge(113) 3×1 spot as a function of reduced temperature $t=|T-T_c|/T_c$ near the critical temperature ($t=0$) is shown in Fig. 7. The transition is much sharper for Ge(113). We have not found any hysteresis in our measurements for both surfaces, which seems to dispel the possibility of a first-order phase transitions. Any small deviation between the cooling and heating cycles disappeared by slowing down the heating rate to $\Delta T/\Delta\tau=0.1$ K min^{-1}. From the changes of the LEED intensity with temperature at temperatures far away from the phase transitions we determined the surface Debye temperature $\theta_s=254$ K for Si(113) and $\theta_s=167$ K for Ge(113).

The spot profiles in Fig. 5 have a Gaussian line shape at low temperature based on statistically distributed defects on the surface and the transfer width of the instrument. Near and above the critical temperature the spot profiles have a Lorentzian-like line shape besides a small asymmetric deviation in the foot. In order to take this deviation into account we measured a spot profile near the critical temperature and used this profile for a fit of the other profiles. With this procedure the shift q became independent of the k range used for the fit. The asym-

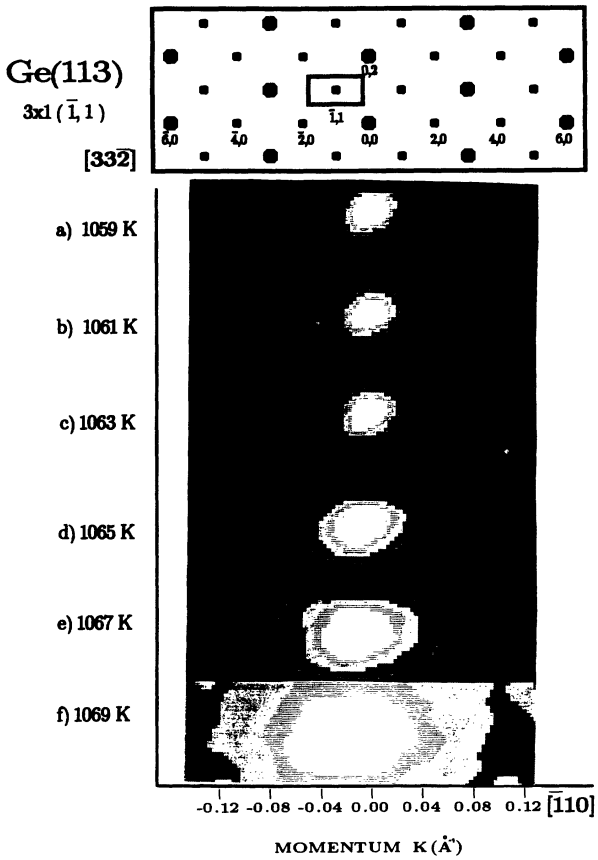

FIG. 6. Two-dimensional LEED intensity plots around the $(\bar{1},1)$ spot as a function of relative momentum K during the (3×1) order-disorder phase transition ($T_c=1063$ K). On top, the location of the two-dimensional window around the $(\bar{1},1)$ spot is given in reciprocal space. The heavy dots represent the 1×1 lattice and the light dots the 3×1 superlattice spots.

metric deviation in the foot had no influence on the full width at half maximum (FWHM). Therefore we used for the evaluation of the FWHM a Lorentzian function according to $I(1+\xi^2(k-q)^2]^{-1}$ where I is the LEED spot intensity and ξ the correlation length. It may be interesting to note that a similar asymmetric line shape has been observed in Monte Carlo simulations of Bartelt, Einstein, and Roelofs[26,27] on a hard hexagon model displaying a transition from the $(3\times1)C$ phase to an IC phase. In that analysis, the deviation from the Lorentzian form has been neglected.

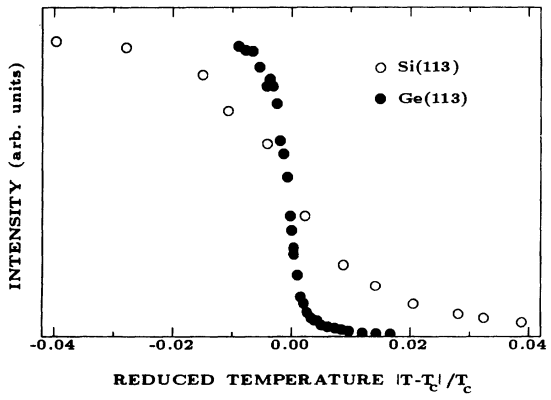

FIG. 7. Si(113) 3×1 and Ge(113) 3×1 LEED $(\bar{1},1)$ spot intensities during the order-disorder phase transition as a function of reduced temperature $|T-T_c|/T_c$.

IV. DISCUSSION

A. Asymmetry and shift of the (3×1) spots

At low temperatures, the (113) 3×1 commensurate surface is expected to take on one of the three physically distinct but equivalent types of domains, characterized by different phase factors.

At and above the C-IC transition, the wave number of the periodicity of the reconstruction changes from $q_C=2\pi/3$ (setting the lattice constant equal to 1) to values $q_{IC}=q_C-q$, leading to a corresponding shift of the (3×1) spots in the LEED pattern. The change can be described in terms of the domains and the domain walls, perpendicular to the $(1\bar{1}0)$ direction, separating different domains. Usually, one distinguishes two types of walls, heavy and light walls, which have been visualized in computer simulations and STM studies (for references, see the review articles[1-5]). By convention, the observed shift of the LEED spots to smaller momentum values, associated with an increase of the periodicity for the reconstruction, is attributed to the presence of heavy walls. Note that heavy and light walls may occur in various modifications, depending on geometrical details of the system and on the kind of microscopic interactions. Modifications include, for instance, superheavy walls and bounded pairs of walls. Obviously, the density of domain walls vanishes as q approaches zero.

The asymmetric broadening of the spot profiles parallel and perpendicular to the $(1\bar{1}0)$ direction at temperatures close to the transition reflects the different behavior of the corresponding correlation lengths. The broader shapes parallel to the $(1\bar{1}0)$ direction reflect the smaller correlation length $\xi_{\parallel}$ in that direction.

B. Different pathways for a commensurate solid to an incommensurate fluid phase

Some years ago, Huse and Fisher[6,7] introduced a new universality class, the chiral melting, describing the transition from a $(3\times1)C$ phase to a disordered IC phase in two dimensions. The three-state chiral clock model is believed to be a prototypical model exhibiting such a transition.[3,7,12] In that model, the clock (or Potts variables), situated on sites i of a rectangular lattice, can take three values $n_i=0,1,2$. In the ordered state, three equivalent types of domains exist just as in the (3×1) commensurate phase. Incommensurate structures may occur due to a chirality parameter Δ which favors one of the two possible types of domain walls. A schematic phase diagram of the three-state chiral clock model is shown in Fig. 8. Interestingly enough, phase diagrams with a similar topology have been discussed for a variety of lattice-gas models with competing interactions describing $(3\times1)C$ phases.[4,13,26-29]

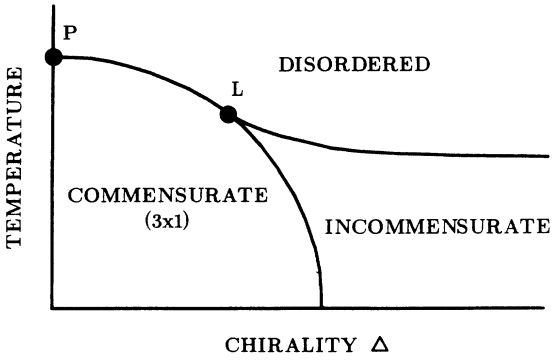

FIG. 8. Schematic phase diagram of the two-dimensional three-state chiral clock model as a function of temperature T and chirality Δ (P: Potts point; L: Lifshitz point).

As seen in Fig. 8, there are typically two pathways, separated by a Lifshitz point, to go from the commensurate 3×1 phase to the disordered phase: (a) via a floating incommensurate phase within a double transition or (b) directly. In case (a), the transition at the lower temperature is of Pokrovsky-Talapov[30] type and the other transition is of the Kosterlitz-Thouless[31] type. Such a floating IC phase has been observed, for instance, for krypton on graphite by Chinn and Fain.[32] The direct transition (b) from the commensurate to the disordered phase is forbidden by the Landau rules for second-order transitions. According to these rules the transition should be of first order. Huse and Fisher pointed out that fluctuations not included in the Landau theory may lead to a continuous transition in the form of the chiral melting. The fingerprint of that transition is the product $(q\xi_{\parallel})$, which has been argued to be constant at the transition, with $\xi_{\parallel}\rightarrow\infty$ and $q\rightarrow0$.[6,7] $\xi_{\parallel}$ is the correlation length parallel to the spatial modulation, i.e., perpendicular to the domain walls. Furthermore, numerical studies, such as finite-size transfer-matrix calculations and Monte Carlo simulation, suggest that the critical exponents are close (or identical) to those of the 2D three-state Potts model, which, in turn, are known exactly.[33]

It should be noted that the existence of a chiral melting has been questioned,[9,10] arguing that, in the case of the chiral clock model, there is a (possibly extremely narrow) floating incommensurate phase at all nonzero values of the chirality parameter Δ. In general, a direct transition from the $(3\times1)C$ phase to the IC disordered phase had to be of first order. Of course, numerical studies as well as experiments can resolve this subtle question only up to a reasonable limit.

The best way to experimentally distinguish between the two different pathways (a) and (b) is to measure the correlation length parallel to the spatial modulation (or perpendicular to the domain walls) $\xi_{\parallel}$, and the shift q in the wave number of the periodicity. Figure 9 exhibits the behavior of these entities for the two different pathways in dependence on temperature. For a double transition there are two different critical temperatures T_{c_1} and T_{c_2} [Fig. 9(a)]; the correlation length $\xi_{\parallel}$ diverges (exponentially[31]) at T_{c_2}, whereas the shift q vanishes (with a square-root power law[30] at T_{c_1}. For a chiral transition there is only one critical temperature where $\xi_{\parallel}$ diverges and q vanishes. The product $(q\xi_{\parallel})$ can be easily distinguished: For a double transition it diverges at T_{c_2}, and for a chiral transition it stays constant approaching T_c.

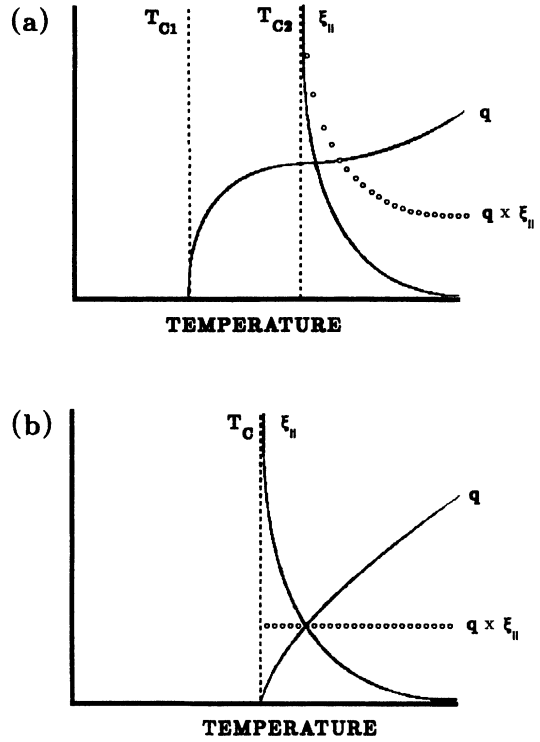

FIG. 9. Shift q of the 3×1 $(\bar{1},1)$ LEED spot and the correlation length $\xi_{\parallel}$ together with the product $q\xi_{\parallel}$ as a function of temperature for two different pathways in the phase diagram given in Fig. 8. For a double transition (a) there are two critical temperatures T_{c_1} and T_{c_2}. $\xi_{\parallel}$ diverges at T_{c_2}, whereas q disappears at T_{c_1} with decreasing temperature. The product $q\xi_{\parallel}$ (open dots) diverges at T_{c_2}. For a chiral transition (b) there is only one T_c and the product of $q\xi_{\parallel}$ (open dots) is constant.

C. Critical exponents

In Fig. 10 we depict our results for the correlation length $\xi_{\parallel}$ and the shift q for (a) Si(113) and (b) Ge(113). We do not find any indication of two different critical temperatures within an uncertainty of 3 K for Si(113) and 0.6 K for Ge(113).

Figure 11 shows the temperature dependence of the product $p=(q\xi_{\parallel})$ for Si(113) (a) and Ge(113) (b) (full dots). In addition, the LEED intensity of the 3×1 spot is depicted. The temperature range was chosen so that the LEED intensity curves look similar for silicon and germanium. For both surfaces there is obviously no indication for a divergent behavior of p. The data may be analyzed to narrow down the maximal extent of the floating IC phase, $\Delta T=T_{c_2}-T_{c_1}$ [see Fig. 9(a)], to $\Delta T<1$ K for Si(113) and to $\Delta T<0.2$ K for Ge(113).

For both surfaces we observe, in some ranges of tem-

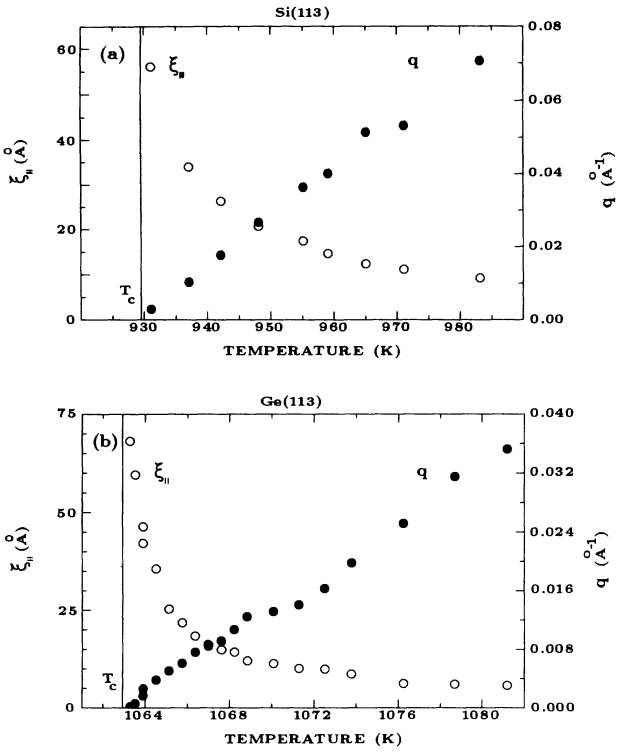

FIG. 10. Shift q (full circles) and correlation length $\xi_{\parallel}$ (open circles) above the transition temperature T_c for Si(113) 3×1 (a) and Ge(113) 3×1 (b).

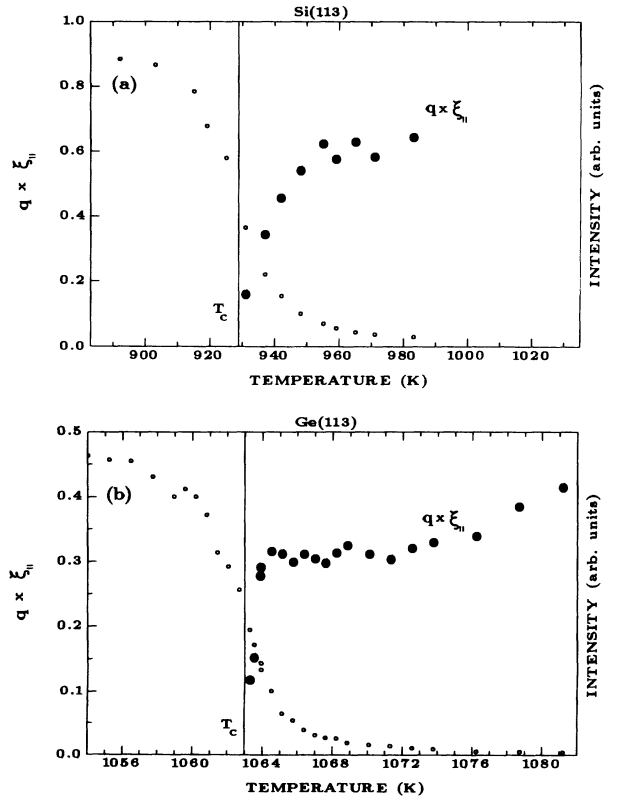

FIG. 11. Temperature dependence of $q\xi_{\parallel}$ (full dots) for Si(113) (a) and Ge(113) (b). The open dots show the temperature dependence of the 3×1 $(\bar{1},1)$ spot intensity.

perature close to the transition, a nearly constant value of $(q\xi_{\parallel})$ as predicted for chiral melting. For Si(113) we get $p\approx0.64$, in agreement with Yang *et al.*[15] For the more perfect, smoother Ge(113) surface the constancy of p is much more evident; see Fig. 11(b). Surprisingly, the value of the constant is approximately half of that for Si(113), $p\approx0.32$.

Note that p has been argued to be a universal constant,[6,7] assuming tacitly, however, fixed dimensionality and a specific type of domain wall. Comparison of the measured values of p to that of the 1D three-state chiral clock model $(p=1/\sqrt{3})$,[7] as has been done by Yang *et al.*[15] in interpreting their result for Si(113), should be viewed with much care. Moreover, the different values of p for Si and Ge may be explained by different types of domain walls; a factor of 2 may be due to pairs of walls or superheavy walls, compared to heavy walls. To substantiate this somewhat speculative explanation, one had to establish the actual positions of the surface atoms and then the structure of the walls.

As seen in Figs. 11(a) and 11(b), the value of p eventually drops down as one approaches T_c more closely. That behavior, which is much less pronounced for Ge, may be attributed to finite-size effects and contamination leading to a reduced correlation length. Indeed, as mentioned above, the size of almost perfect surface areas is larger for Ge(113) (linear extent of about 370 Å) than for Si(113) (about 250 Å). However, other explanations of the drop are possible, including, especially for Si, a possible inconsistency with the theory of critical melting.

The critical exponents $\nu_{\parallel}$ and $\nu_{\perp}$ were taken from $\log_{10}$-$\log_{10}$ plots of the experimental data for $\xi_{\parallel}$ and $\xi_{\perp}$ (see Fig. 12) in the temperature range of $1063.5<T<1071$ K for $\xi_{\parallel}$ and $1065<T<1071$ K for $\xi_{\perp}$. From our experimental data, it follows that $\nu_{\parallel}$, the critical exponent of the correlation length parallel to the direction of modulation, $\xi_{\parallel}\sim|T-T_c|^{-\nu_{\parallel}}$, has about the same value as $\nu_{\perp}$, the critical exponent for the correlation length in the perpendicular direction. This isotropic scaling may be seen directly from the fact that the ratio $\xi_{\perp}/\xi_{\parallel}$ is, nearly, independent of temperature close to T_c, as shown in Fig. 12 for Ge(113), with $\xi_{\perp}/\xi_{\parallel}\approx2$.

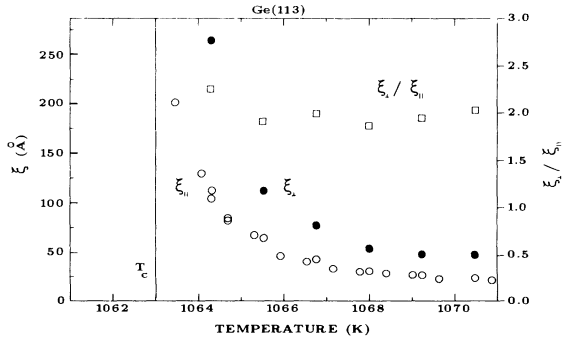

FIG. 12. Temperature dependence of the correlation length $\xi_{\parallel}$ (open dots) and $\xi_{\perp}$ (full dots) during the (3×1) order-disorder phase transition on Ge(113). The ratio $\xi_{\perp}/\xi_{\parallel}$ (open squares) is also given.

For the values of the critical exponents of the correlation lengths we found, in the case of Ge, $\nu_{\parallel}=0.72\pm0.05$ and $\nu_{\perp}=0.71\pm0.10$, with $T_c=1063.0\pm0.5$ K. The critical temperature has been also determined from the data for the correlation length. The estimates for ν are rather close to the value for the three-state Potts model, $\nu=\frac{5}{6}$.[33] For Si(113), we obtained $T_c=929\pm3$ K and $\nu_{\parallel}=0.75\pm0.10$ [$\nu_{\perp}$ has not been measured for Si(113)].

In the prior LEED study on silicon,[15] $\xi_{\perp}$ could not be measured because of the limited instrumental resolution. The estimate for $\nu_{\parallel}$ was somewhat higher than in our case, with a rather large error bar, $\nu_{\parallel}=0.99\pm0.18$. Numerical calculations on models exhibiting (supposedly) chiral melting yielded isotropic scaling with values for ν of about 0.8–0.9,[12,13,27] in reasonable agreement with our estimates. Note that in all cases the critical exponents are effective ones and estimates are affected in various ways, such as corrections to scaling, finite-size effects, and uncertainties in T_c.

The critical exponent β of the shift in the wave number, $q\sim|T-T_c|^{\bar{\beta}}$, was estimated to be $\bar{\beta}=0.77\pm0.05$ in the case of Ge and $\bar{\beta}=0.99\pm0.10$ in the case of Si. Obviously, the product $p=(q\xi_{\parallel})$ is constant close to T_c only if $\nu_{\parallel}=\bar{\beta}$. This identity is satisfied quite well for Ge, in contrast to the situation for Si. Indeed, the rather pronounced drop of p close to T_c [see Fig. 11(a)], may be traced back to the rather large value of $\bar{\beta}$.

We also determined the canonical critical exponents of the order parameters, β, and of the susceptibility, γ, from standard $\log_{10}$-$\log_{10}$ plots. Figure 13 shows a $\log_{10}$-$\log_{10}$ plot of the LEED intensities as a function of the reduced temperature for germanium. The slopes of these $\log_{10}$-$\log_{10}$ plots determine the effective critical exponents γ ($T>T_c$) and β ($T<T_c$). We used the temperature range between $\log_{10}$-$\log_{10}\sim-3.2$ and $\ln t\sim-1.8$ in order to estimate the critical exponents. Closer to T_c, finite-size and contamination effects are expected to play a major role; further away from T_c, corrections to scaling may dominate. As results we obtained $\gamma=1.27\pm0.10$ and $\beta=0.10\pm0.01$, which may be compared to the values for the 2D three-state Potts model, $\beta=\frac{1}{9}$ and $\gamma=\frac{13}{9}$.[33] The Potts values for β and γ are indicated by the solid lines in Fig. 13.

For Si(113) we obtained $\gamma=1.20\pm0.20$ and $\beta=0.093\pm0.02$, in reasonable agreement with the prior estimates by Yang *et al.*,[15] $\gamma=1.03\pm0.19$ and $\beta=0.11\pm0.04$. Monte Carlo simulations yielded in those parts of the phase diagram where chiral melting is expected estimates of[8] β and[27] γ which are compatible with the Potts values. We should emphasize that we always estimated the values of *effective* exponents, which, of course, may deviate from the true asympototic ones. In the experimentally accessible range of reduced temperatures t the correlation length increases up to a few hundred angstroms. Therefore the experimental data correspond, e.g., to simulational data on systems with the linear dimension of the order of 100 lattice spacings. Usually, such moderate sizes seem to be sufficient to extract rather decent values for the exponents; see, e.g., Refs. 8, 26, and 27. Certainly it would be desirable to obtain meaningful data even closer to T_c, but one has to be aware of finite-size and contamination effects. Furthermore, more accurate estimates are limited by uncertainties in determining the transition temperature very accurately.

D. Comparison of integral intensities from LEED and SPA-LEED

We measured integrated LEED intensities $I(T)$ with a low-resolution LEED system (Varian) to determine the critical exponent α. This method was introduced by Bartelt, Einstein, and Roelofs,[34] who argued that the integrated intensity is expected to have the form $I(T)=A\mp B_{\pm}|t|^{1-\alpha}-Ct$; $t=|T-T_c|/T_c$, where A, B and C are fit parameters. In Fig. 14, the integrated LEED intensities are compared to those of the prior study.[15] The integrated LEED intensities of Yang *et al.* drop down less steeply close to the critical temperature

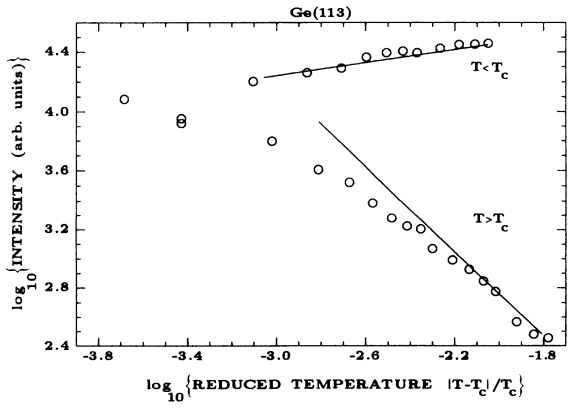

FIG. 13. $\log_{10}$-$\log_{10}$ plots of the LEED intensity for Ge(113) as a function of reduced temperature $|T-T_c|/T_c$ below and above T_c. The solid lines are drawn using slopes according to the universality class of the three-state Potts model.

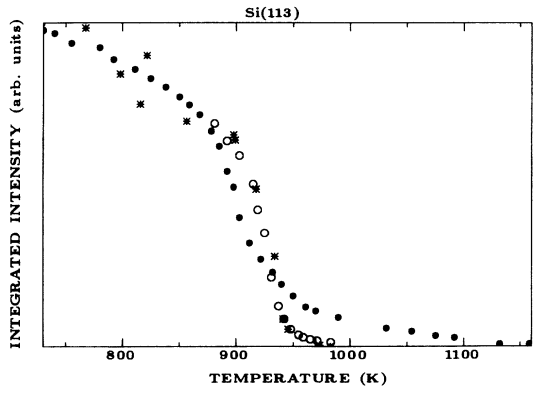

FIG. 14. Comparison of the integrated LEED intensities of a 3×1 spot measued by Yang *et al.* Ref. (15) (full dots) and our results (stars) both measured with conventianal low-resolution LEED systems. In addition, our high-resolution SPA-LEED results are shown (open dots)

than our data, which may reflect stronger finite-size and contamination effects than in our data. Unfortunately, estimates for α depend strongly on the integration radius for the LEED spots. For example, the estimated values for α by Yang *et al.* varied between 0.26 and 0.64. Using a variable integration radius (four times the FWHM, we obtained values between 0.6 and 0.8, both for Ge and Si. These values should be viewed with much care, having in mind the ambiguities of the method and general difficulties to determine the critical exponent of the specific heat accurately from data which may be not sufficiently close to T_c. Obviously, our values are appreciably higher than $\frac{1}{3}$, the exact number for the three-state Potts model.

We measured the integrated LEED intensities also with the high-resolution SPA-LEED, as included in Fig. 14 and found, somewhat surprisingly, the same temperature dependence as with the low-resolution LEED system.

E. Recent study of Si(113)

Very recently, Mochrie and co-workers[24,35] studied the Si(113) (3×1) order-disorder phase transition, using x-ray scattering. At about 960 K, Abernathy *et al.*[35] observed the incommensurate-to-incommensurate transition, characterized by a divergent correlation length and appearance of domain walls, in agreement with our observations on a direct continuous *C*-IC transition. Close to T_c, they found the product $p=(q\xi_{\parallel})$ to be constant, apart from a weak oscillation. It may be interesting to note that we observed a similar oscillation for a contaminated Ge(113) sample, but not in the case of a more cleanly prepared surface. At any rate, results are compatible with chiral melting, postulating a constant for p near T_c.

To elucidate the nature of the transition, Abernathy *et al.* also estimated various critical exponents. As in the LEED analyses, β (=0.11±0.02) and γ (=1.56±0.13) are compatible with the values of the three-state Potts universality class (albeit, the LEED studies gave somewhat smaller estimates for γ). However, in contrast to our result for Ge, the exponent for the correlation length perpendicular to the domain walls, $\nu_{\parallel}$ (=0.65±0.07), is found to be different from that for the correlation length parallel to the domain walls, $\nu_{\perp}$ (=1.05±0.07). This anisotropic scaling could be due to the closeness of the Lifshitz point, at which one expects $\nu_{\parallel}=\frac{2}{3}$ and $\nu_{\perp}=1$.[11,24] Unfortunately, in the case of Si, we determined only $\nu_{\parallel}$ (in good agreement with the x-ray result). For Ge, we observe isotropic scaling, in accordance with simulational and numerical findings on chiral melting.

V. CONCLUSION

We measured the commensurate-incommensurate (3×1) order-disorder phase transition at Ge(113) and Si(113) surfaces. The characteristics of the transitions are compared to chiral melting, as has been discussed for various microscopic models with competing interactions.

The crucial criterion of a constant value for the product of the shift in the wave number, describing the spatially modulated structure, and the correlation length perpendicular to the domain walls seems to be well satisfied for Ge, while the situation is not as clear in Si. A possible difference of the constant by a factor of 2 may be explained by different types of domain walls in Ge and Si.

The critical exponents of the order parameter β and of the susceptibility γ are rather close to those of the two-dimensional three-state Potts model, in agreement with theoretical work on chiral melting. Using integrated LEED intensities to determine the exponent of the specific heat, α, somewhat ambiguous results are obtained.

TABLE I. Critical exponents α β, γ, $\nu_{\parallel}$, $\nu_{\perp}$, and $\bar{\beta}$ (see text), the product $q\xi_{\parallel}$ of shifts q of the 3×1 LEED spots and the correlation length $\xi_{\parallel}$ parallel to the corrugation introduced through domain walls, the ratio $\xi_{\perp}/\xi_{\parallel}$, and the transition temperature T_c for the 3×1 order-disorder phase transition of the Ge(113) and Si(113) surfaces. Our experimental values are compared to the data of Yang *et al.* (Ref. 15) and Abernathy *et al.* (Ref. 35). Also given are theoretical values for the three-state Potts model.

	α	β	γ	$\nu_{\parallel}$	$\nu_{\perp}$	$\bar{\beta}$	$q\xi_{\parallel}$	$\xi_{\perp}/\xi_{\parallel}$	T_c (K)
Three-state Potts	0.333	0.111	1.44	0.833	0.833				
Ge(113)	0.71	0.10	1.27	0.72	0.71	0.77	0.32	2.0	1063
	±0.1	±0.01	±0.10	±0.05	±0.10	±0.05	±0.05	±0.1	±10
Si(113)	0.71	0.093	1.20	0.75		0.99	0.64		929
	±0.1	±0.02	±0.20	±0.1		±0.1	±0.1		±20
Si(113)	0.32	0.11	1.03	0.99			0.577		844
(Yang *et al.*)	±0.06	±0.04	±0.19	±0.18					
Si(113)		0.11	1.56	0.65	1.06	0.66	1.6		959
(Abernathy *et al.*)		±0.02	±0.13	±0.07	±0.07	±0.05	±0.2		

For Ge, considering correlation lengths parallel and perpendicular to the domain walls, isotropic scaling is observed. In contrast, a recent x-ray-scattering study suggests anisotropic scaling for Si, possibly reflecting the closeness of a Lifshitz point.

The critical exponents from our work and from the literature are summarized in Table I. Further experimental work and theoretical modeling on these fascinating surfaces seem desirable.

Note added in proof. Very recently, we repeated and extended our experiments on silicon to study the question of anisotropic scaling, reported by Abanathy *et al.*[35] We used a Si(113) wafer and also improved the temperature resolution. We found, for the new sample, a somewhat higher transition temperature ($T_c = 963 \pm 20$ K). We suppose that, due to the fact that wafer domains of larger size can be prepared: the shift in T_c may be, therefore, partly regarded as a finite-size effect. The value for the critical exponent $\nu_\parallel$ agreed with our values given in Table I. However, we found $\nu_\perp < \nu_\parallel$ (indicating, possibly, insufficient resolution), similar to the result by Yang *et al.*[15]

ACKNOWLEDGMENTS

We thank Professor G. Ertl for support and Dr. R. Schuster for discussions. We are also grateful to P. Geng for his skillful technical assistance. We thank Professor S. Mochrie for informing us about the x-ray-scattering study on Si(113) prior to publication. This work was supported by the Deutsche Forschungsgemeinschaft through SFB 6.

*Institut für Festkörperforschung, Forschungszentrum Jülich, P.O. Box 1913, D-52425 Jülich, Germany.

[1]M. Schick, Prog. Surf. Sci. **11**, 245 (1981).
[2]M. E. Fisher, J. Stat. Phys. **34**, 667 (1984).
[3]M. den Nijs, in *Phase Transitions and Critical Phenomena,* edited by C. Domb and J. L. Lebowitz (Academic, London, 1988), Vol. 12, p. 219.
[4]W. Selke, in *Phase Transitions and Critical Phenomena,* edited by C. Domb and J. L. Lebowitz (Academic, London, 1992), Vol. 15.
[5]B. N. J. Persson, Surf. Sci. Rep. **15**, 1 (1992).
[6]D. A. Huse and M. E. Fisher, Phys. Rev. Lett. **49**, 793 (1982).
[7]D. A. Huse and M. E. Fisher, Phys. Rev. B **29**, 239 (1984).
[8]W. Selke and J. M. Yeomans, Z. Phys. B **46**, 311 (1982).
[9]F. D. M. Haldane, P. Bak, and T. Bohr, Phys. Rev. B **28**, 2743 (1983).
[10]H. J. Schulz, Phys. Rev. B **28**, 2746 (1983).
[11]S. Howes, L. P. Kadanoff, and M. den Nijs, Nucl. Phys. B **215**, 169 (1983).
[12]P. M. Duxbury, J. Yeomans, and P. D. Beale, J. Phys. A **17**, L179 (1984).
[13]E. Domany and B. Schaub, Phys. Rev. B **29**, 4095 (1984).
[14]H. U. Everts and H. Röder, J. Phys. A **22**, 2475 (1989).
[15]Y. N. Yang, E. D. Williams, R. L. Park, N. C. Bartelt, and T. L. Einstein, Phys. Rev. Lett. **64**, 2410 (1990).
[16]U. Myler and K. Jacobi, Surf. Sci. **220**, 253 (1989).
[17]U. Myler, P. Althainz, and K. Jacobi, Surf. Sci. **251/252**, 607 (1991).
[18]K. Jacobi and U. Myler, Surf. Sci. **284**, 223 (1993).
[19]R. Heckingbottom and P. R. Wood, Surf. Sci. **437**, 23 (1970).
[20]B. Z. Olshanestsky and V. I. Mashanov, Surf. Sci. **414**, 111 (1981).
[21]Y. R. Xing, J. P. Zhang, J. A. Wu, C. Z. Liu, and C. H. Wang, Surf. Sci. Lett. **L215**, 232 (1990).
[22]J. Knall, J. B. Pethica, J. D. Todd, and J. H. Wilson, Phys. Rev. Lett. **1733**, 66 (1991).
[23]M. J. Hadley, S. P. Tear, B. Röttger, and H. Neddermeyer, Surf. Sci. **258**, 280 (1993).
[24]S. G. J. Mochrie (private communication).
[25]B. Z. Olshanetsky, V. I. Mashanov, and A. I. Nikiforov, Surf. Sci. **111**, 429 (1981).
[26]N. C. Bartelt, T. L. Einstein, and L. D. Roelofs, Phys. Rev. B **35**, 1776 (1987).
[27]N. C. Bartelt, T. L. Einstein, and L. D. Roelofs, Phys. Rev. B **35**, 4812 (1987).
[28]W. Selke, W. Kinzel, and K. Binder, Surf. Sci. **125**, 74 (1983).
[29]R. Schuster, J. V. Barth, G. Ertl, and R. J. Behm, Phys. Rev. B **44**, 13689 (1991).
[30]V. L. Pokrovsky and A. I. Talapov, Phys. Rev. Lett. **42**, 65 (1979).
[31]J. M. Kosterlitz and D. J. Thouless, J. Phys. C **6**, 1181 (1973).
[32]M. D. Chinn and S. C. Fain, Jr., Phys. Rev. Lett. **39**, 146 (1977).
[33]F. Y. Wu, Rev. Mod. Phys. **54**, 235 (1982).
[34]N. C. Bartelt, T. L. Einstein, and L. D. Roelofs, Phys. Rev. B **32**, 2993 (1985).
[35]D. L. Abernathy, R. J. Birgeneau, K. I. Blum, and S. G. J. Mochrie, Phys. Rev. Lett. **71**, 750 (1993).

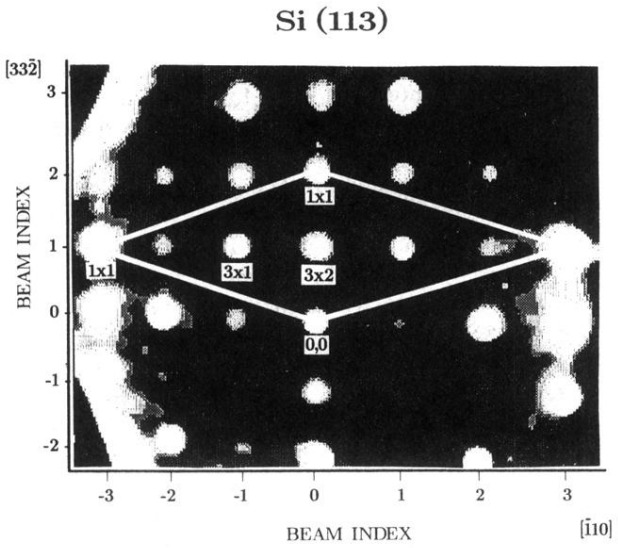

FIG. 1. LEED pattern of the 3×2 reconstructed Si(113) surface at room temperature ($E_p=60$ eV) using a spot-profile-analysis system LEED (SPA-LEED).

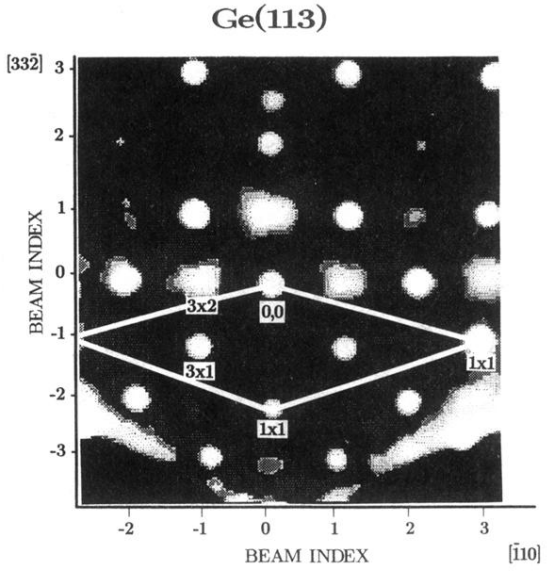

FIG. 2. LEED pattern of the 3×2 reconstructed Ge(113) surface at about 120 K ($E_p = 50$ eV). The 3×2 spots are three times broader and weaker than for the Si(113) surface.

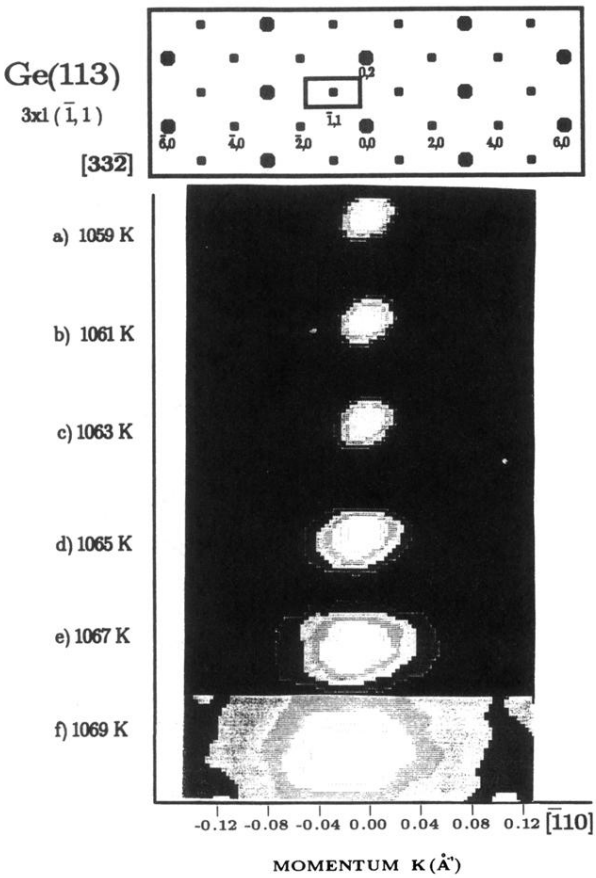

FIG. 6. Two-dimensional LEED intensity plots around the $(\bar{1},1)$ spot as a function of relative momentum K during the (3×1) order-disorder phase transition ($T_c = 1063$ K). On top, the location of the two-dimensional window around the $(\bar{1},1)$ spot is given in reciprocal space. The heavy dots represent the 1×1 lattice and the light dots the 3×1 superlattice spots.